J Mater Sci (2011) 46:3282–3290
DOI 10.1007/s10853-010-5215-8

Characterization of the evolution of recrystallization by fluctuation and fractal analyses of the magnetic hysteresis loop in a cold rolled non-oriented electric steel

Francisco E. da Silva · Francisco Nelio C. Freitas · Hamilton Ferreira G. Abreu · Lindberg L. Gonçalves · Elineudo P. de Moura · Manoel R. Silva

Received: 23 November 2010 / Accepted: 22 December 2010 / Published online: 6 January 2011

Abstract Silicon steels with non-oriented grains are widely used in the fabrication of electrical motor nucleus where a low magnetic loss is an important point. The performance of these motors is affected by the level of recrystallization of these steels which can come from the steel plant in a semi-processed condition. In this condition, they have a partially deformed structure and are submitted to an adequate annealing heat treatment, after reaching the end shape, to get an appropriate magnetic property. In this study, samples of an electric steel, cold rolled 50% in thickness, were withdrawn during the industrial heat treatment at temperatures of 575, 580, 600, 620 and 730 °C with the objective of evaluating the evolution of recrystallization with temperature. Magnetic properties were measured at room temperature in a vibrating sample magnetometer and the changes in magnetic hysteresis loop with temperature have been identified by using two pattern classification techniques, principal-component analysis and Karhunen-Loève (KL) expansion, associated with statistical fluctuations and fractal analyses. The fluctuation and fractal analyses were used as preprocessing tools of the series which are built from each hysteresis loop, properly renormalized, whose values correspond to the amplitudes of the loop at given equally spaced values of the renormalized field interpolated between the experimental data. The samples have been classified in four sets corresponding to different temperatures, and to samples without annealing heat treatment and recrystallized ones. The classification of the different microstructures have been obtained by applying the two pattern classification techniques to the vectors obtained from the preprocessing, and in particular a 100% success rate has been reached by using KL expansion.

F. E. da Silva · F. N. C. Freitas · H. F. G. Abreu · L. L. Gonçalves (✉) · E. P. de Moura
Departamento de Engenharia Metalúrgica e de Materiais, Universidade Federal do Ceará, Campus do Pici, Bloco 714, Fortaleza, CE 60455-760, Brazil
e-mail: lindberg@fisica.ufc.br

M. R. Silva
Departamento de Física e Química, Instituto de Ciências Exatas, Universidade Federal de Itajubá, Itajubá, MG 37500-903, Brazil

Introduction

The main destination of non-oriented-grain electric steel is the market for electrical rotating machines such as engines and compressors, in which the direction of magnetization rotates 60° every cycle, but always remains in the plane of the plate.

Semi-processed electrical steels have a partially deformed structure and are submitted to the final annealing process after reaching the end shape. An adequate annealing heat treatment is important to get an appropriate recrystallization texture and consequently improve magnetic properties.

The magnetic properties of non-oriented silicon steel are strongly dependent on recrystallization and grain size [1, 2]. Changes in texture during recrystallization influence hysteresis loops. The energy loss per unit volume for each cycle of magnetization is equal to the area of the hysteresis loop [3]. The area inside the hysteresis curve gives a quantitative value of the loss of magnetic energy per unit volume in the material, because larger the area greater the magnetic loss, and vice versa. Monitoring the magnetic losses can be an alternative technique to monitor the process of recrystallization. The difficulty, however, is the

small variation of the area within the hysteresis loop when small temperature gradients are studied. Consequently, from the results obtained for the magnetic energy loss we have been unable to discriminate the different stages of the recrystallization process.

The use of residual magnetization and coercivity as discriminators for this process has also been shown to be ineffective in identifying the variation of the recrystallization with temperature.

These results led us to conclude that to have the magnetic hysteresis loop as a discriminator of the different stages of the recrystallization, more information on it had to be associated. To this aim we have treated all the relevant information contained in the hysteresis loop associated with two pattern classification techniques, namely, principal-component analysis (PCA) and Karhunen-Loève (KL) expansion, associated with the statistical fluctuations obtained by means of Hurst and detrended-fluctuation analyses (DFA), and fractal analyses carried out by applying the minimal cover and box-counting techniques. The application of these pattern classification techniques in the preprocessed data of the hysteresis loops with the aim to detect the various stages of the recrystallization is the main objective of this article. To this end, we present in the next section a description of the materials, the experimental procedures and the experimental results. A brief review of the pattern classification techniques and numerical analysis used in the treatment of the data are presented in 'Pattern-classification tools' and 'Statistical fluctuation and fractal analyses', respectively. Finally, the results are presented and discussed in 'Results and discussion', and the main conclusions of the article are summarized in the 'Conclusions'.

Materials and experimental measurements

Samples and measurements

The composition of the studied steel is shown in Table 1.

The steel was cold rolled 50% in the thickness of the plate in an industrial rolling process. After cold rolling, material was subjected to annealing in a box at a temperature of 730 °C (soaking temperature) for 12 h. Before reaching that temperature, steel soaking samples were taken at temperatures of 575, 580, 600, 620 and 730 °C, with the aim of analyzing the partial recrystallization in the microstructure of the material.

Table 1 Chemical composition of steel electrical non-oriented

Elements	C	Si	P	S	Al	Mn	Fe
% (mass)	0.050	1.280	0.025	0.014	0.036	0.290	Bal.

The EBSD was used to follow recrystallization volume fraction evolution. Samples were ground with grit sizes of 100, 220, 320, 400, 600 and 1200 and polished with diamond paste of 6, 3 and 1 μm before silica colloidal final preparation. A Philips XL-30 scanning electron microscope equipped with an Oxford-Inca Crystal EBSD system was used to get patterns.

Five hysteresis curves for each temperature were measured in a vibrating sample magnetometer. A maximum field of 10,000 Oe was applied during measurement.

Experimental results

With the help of EBSD it is possible not only to determine the orientation of each grain individually (microtexture), but also the difference in orientation between each grain and its neighbours (mesotexture). This misorientation between each grain is the tool to calculate the recrystallized volume fraction of the samples. Figure 1 shows the recrystallized fraction measured by EBSD, considering as recrystallized grains that have no sub-grains with misorientations less than 5° inside. After reaching the temperature of 595 °C, there is sharp change in the recrystallized fraction.

In a graph $B \times H$, B being magnetic induction and H being the magnetic field intensity, the loss is the area of hysteresis cycle (hc). Figure 2 shows one cycle of hysteresis for a sample cold rolled. This sample is expected to have the highest value of magnetic loss. As already pointed out, the area inside the loop is very small, as can be seen in Fig. 2b, where it is shown a zoom of the central area of looping. The size of central area makes it very difficult to use conventional procedures to follow the evolution of losses during recrystallization process.

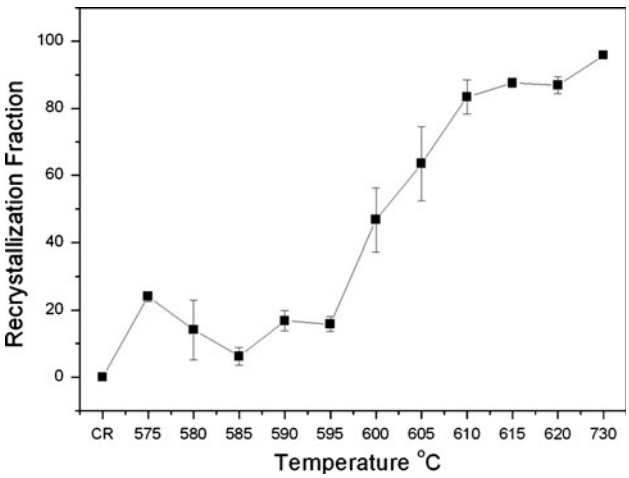

Fig. 1 Evolution of recrystallization fraction with temperature measured by EBSD

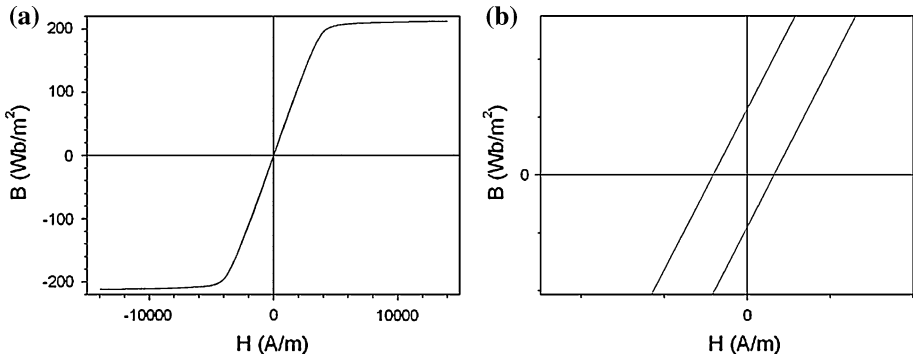

Fig. 2 Hysteresis loop for a sample cold rolled (**a**); zoom in the central region of hysteresis loop (**b**)

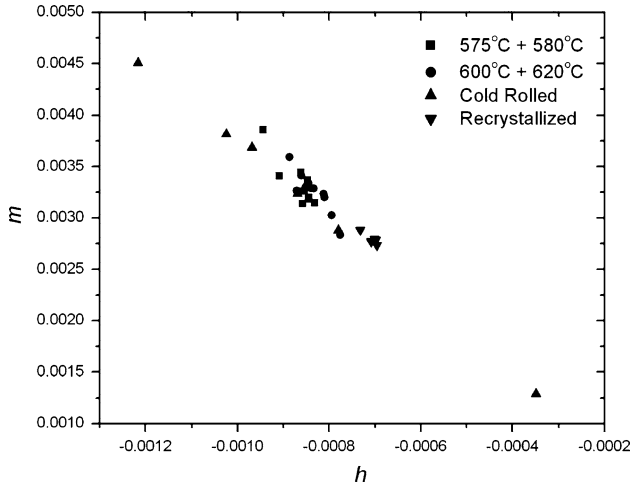

Fig. 3 Renormalized residual magnetization and coercivity at different temperatures

In Fig. 3 we show the residual magnetization (m) and coercivity (h) renormalized by the saturation magnetization and saturation magnetic field, respectively, for the different samples and temperatures. As it can be seen, no discrimination can be achieved by using these two parameters, as it was observed in the introduction. Therefore, we have to consider all additional information contained in the magnetic hysteresis loop to obtain the desired discrimination of the stages of crystallization at different temperatures.

Pattern-classification tools

The first step towards the introduction of the classification scheme is to renormalize the hysteresis loop, $m(h)$, where $m = \mathrm{M(H)/M_S}$ and $h = \mathrm{H/H_S}$, to define a single metric in the process. From these curves we can make use of standard pattern-recognition tools to group the hysteresis loops according to relevant classes. The next step towards classification is to build feature vectors from these curves, whose components are the amplitude of the loop at given values of the renormalized field. Therefore, by considering the dimension of the vector space equal to n, one can define the column vector $\mathbf{X}_i$ associated to the ith loop as

$$\mathbf{X}_i = \begin{pmatrix} x_i(h_i) \\ x_i(h_2) \\ \vdots \\ x_i(h_n) \end{pmatrix} \equiv \begin{pmatrix} m_i^+(h_1) - m_i^-(h_1) \\ m_i^+(h_2) - m_i^-(h_2) \\ \vdots \\ m_i^+(h_n) - m_i^-(h_n) \end{pmatrix}, \quad (1)$$

where $m_i^+(h_j) - \left[m_i^-(h_j)\right]$ denotes the upper (lower) branch of the hysteresis loop. In our studies, we have chosen n as equal to the number of experimental points (187), and they have been determined by interpolation procedures to guarantee that amplitude series for the different hysteresis loops were obtained at identical values of the field. In the following subsections we present the methods we will use to group feature vectors into relevant classes, namely, PCA and KL transformation [4]. This procedure has to be repeated for many distinct choices of training and testing vectors, as a way to evaluate the average efficiency of the classifier. One can then study the resulting confusion matrices, which report the percentage of vectors of a given class assigned to each of the possible classes.

PCA

Given a set of N feature vectors $\{\mathbf{x}_i\}$, PCA [4] is based on the projection of those vectors onto the directions defined by the eigenvectors of the covariance matrix

$$\mathbf{S} = \frac{1}{N}\sum_{i=1}^{N}(\mathbf{x}_i - \bar{\mathbf{x}})(\mathbf{x}_i - \bar{\mathbf{x}})^{\mathrm{T}} \quad (2)$$

in which $\bar{\mathbf{x}}$ is the average vector,

$$\bar{\mathbf{x}} = \frac{1}{N}\sum_{i=1}^{N}\mathbf{x}_i \quad (3)$$

and T denotes the transpose vector. If the eigenvalues of $\mathbf{S}$ are arranged in decreasing order, the projections along the first eigenvector, corresponding to the largest eigenvalue, define the first principal component, and account for the largest variation of any linear function of the original

variables. In general, the *n*th principal component is defined by the projections of the original vectors along the direction of the *n*th eigenvector. Therefore, the principal components are ordered in terms of the (decreasing) amount of variation of the original data for which they account.

Thus, PCA amounts to a rotation of the coordinate system to a new set of orthogonal axes, yielding a new set of uncorrelated variables, and a reduction on the number of relevant dimensions, if one chooses to ignore principal components whose corresponding eigenvalues lie below a certain limit.

A classifier based on PCA can be built by using the first few principal components to define modified vectors, whose class averages are determined from the vectors in the training group. Then, a testing or a training vector $\mathbf{x}_i$ is assigned to the class whose average vector lies closer to $\mathbf{x}_i$ within the transformed space. This is known as the nearest-class-mean rule, and would be optimal if the vectors in different classes followed normal distributions.

KL transformation

Let $\mathbf{x}_i$ be the vector corresponding to the *i*th loop. The KL transformation [4] consists of first projecting the training vectors along the eigenvectors of the within-class covariance matrix $\mathbf{S}_\mathrm{W}$, defined by

$$\mathbf{S}_\mathrm{W} = \frac{1}{N}\sum_{k=1}^{N_\mathrm{c}}\sum_{i=1}^{N_\mathrm{k}} y_{ik}(\mathbf{x}_i - \bar{\mathbf{x}}_k)(\mathbf{x}_i - \bar{\mathbf{x}}_k)^\mathrm{T}, \tag{4}$$

where N_c is the number of different classes, N_k is the number of vectors in class k, $\bar{\mathbf{x}}_k$ is the average vector of class k and T denotes the transpose of a matrix (in this case, of a column vector). The element y_{ik} is equal to one if x_i belongs to class k, and zero otherwise.

We also rescale the resulting vectors by a diagonal matrix built from the eigenvalues λ_j of $\mathbf{S}_\mathrm{W}$. In matrix notation, this operation can be written as

$$\mathbf{X}' = \Lambda^{-\frac{1}{2}}\mathbf{U}^\mathrm{T}\mathbf{X}, \tag{5}$$

where $\mathbf{X}$ is the matrix whose columns are the training vectors, $\mathbf{x}_i$, $\Lambda = \mathrm{diag}(\lambda_1; \lambda_2; \ldots)$, and $\mathbf{U}$ is the matrix whose columns are the eigenvectors of $\mathbf{S}_\mathrm{W}$. This choice of coordinates makes sure that the transformed within-class covariance matrix corresponds to the unit matrix. Finally, to compress the class information, we project the resulting vectors onto the eigenvectors of the between-class covariance matrix $\mathbf{S}_B$,

$$\mathbf{S}_\mathrm{B} = \frac{1}{N}\sum_{k=1}^{N_\mathrm{c}}\frac{N_k}{N}(\bar{\mathbf{x}}_k - \bar{\mathbf{x}})(\bar{\mathbf{x}}_k - \bar{\mathbf{x}})^\mathrm{T}, \tag{6}$$

where $\bar{\mathbf{x}}$ is the overall average vector. The full transformation can be written as

$$\mathbf{X}'' = \mathbf{V}^\mathrm{T}\Lambda^{-\frac{1}{2}}\mathbf{U}^\mathrm{T}\mathbf{X},$$

where $\mathbf{V}$ is the matrix whose columns are the eigenvectors of $\mathbf{S_B}$ (calculated from $\mathbf{X}'$).

Statistical fluctuation and fractal analyses

The following subsections describe the methods of fluctuation and fractal analyses employed as a preprocessing step in the classification scheme. These methods are usually employed to identify long-term memory effects in self-affine (or fractal) time series. In a time series of genuine fractal nature, memory effects can be gauged by a single number η which relates a measure of the average fluctuations $Q(\tau)$ inside the time series to the size τ of the time window used in the calculation, according to the power law

$$Q(\tau) \sim \tau^{\eta}. \tag{8}$$

For an experimental time series (not necessarily a time series), which of course cannot be genuinely fractal, the various analyses described below have proved to be nevertheless quite useful in providing signatures of the underlying processes peculiar to distinct situations, such as different defects present in welding joints, probed by ultrasonic techniques [5], as well as different defects in gearboxes, as registered by vibration signals [6].

Each technique then involves the calculation of the average of the functions $Q(\tau)$ over all cells, for a defined set of values of τ, which will be used to characterize the different microstructure since the exponents η are not sufficient to produce the desired discrimination.

Hurst (or *R*/*S*) Analysis

The rescaled-range (*R*/*S*) analysis was introduced by Hurst [7] as a tool for evaluating the persistence or antipersistence of a time series. The method works by dividing the series into intervals of a given size τ, and calculating the average ratio *R*/*S* of the range (the difference between the maximum and minimum values of the series) to the standard deviation inside each interval. The size τ is then varied, and a curve of the rescaled range R/S as a function of τ is obtained.

Mathematically, the *R*/*S* analysis is defined in the following way. Given an interval of size τ, whose left end is located at point i_0, we calculate the average of the time series z_i inside the interval,

$$\langle z \rangle = \frac{1}{\tau}\sum_{i=i_n}^{i_0+\tau-1} z_i \tag{9}$$

then define an accumulated deviation from the mean as

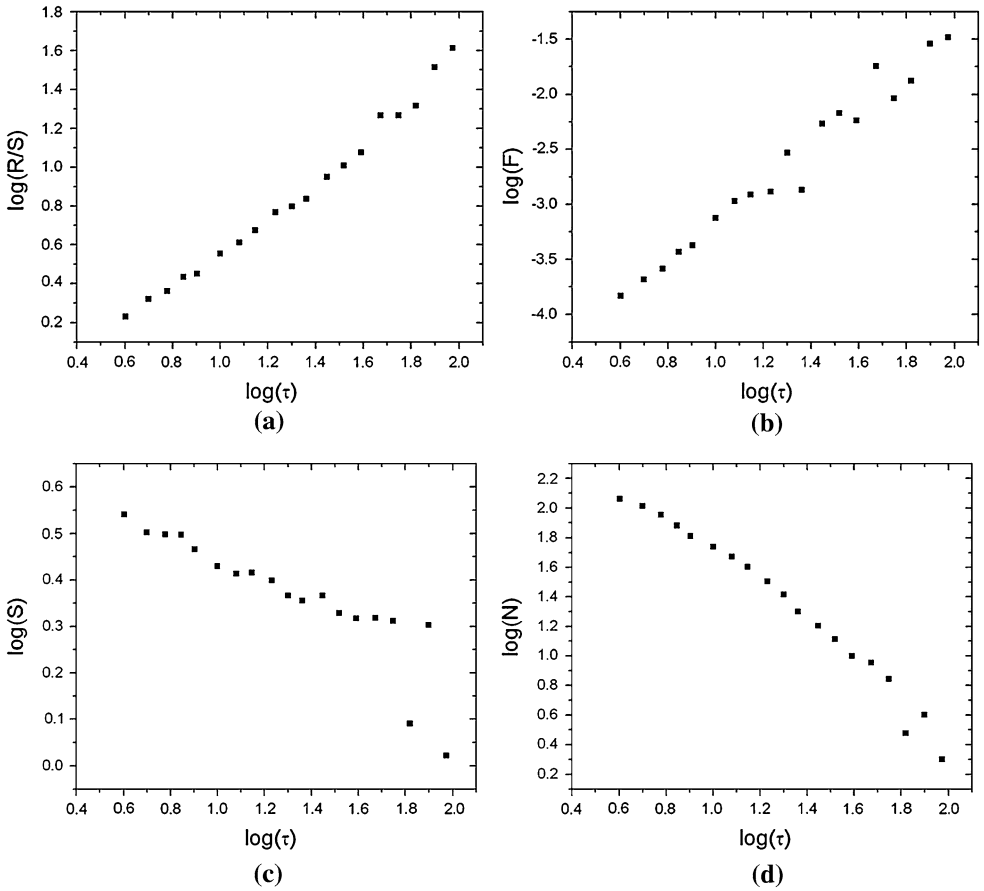

Fig. 4 Typical curves obtained from the fractal analyses. **a** RS analysis, **b** DF analysis, **c** MC analysis, **d** BC analysis

$$Z_i = \sum_{k=i_0}^{i} \left(z_k - \langle z \rangle_\tau\right) \tag{10}$$

from which we extract a range

$$R(\tau) = \max_{i_0 \le i \le i_0+\tau-1} Z_i - \min_{i_0 \le i \le i_0+\tau-1} Z_i \tag{11}$$

and the corresponding standard deviation,

$$S(\tau) = \sqrt{\frac{1}{\tau}\sum_{i=i_0}^{i_0+\tau-1} \left(z_k - \langle z \rangle_\tau\right)^2} \tag{12}$$

Finally, we obtain the rescaled range $R_S(\tau) = R(\tau)/\mathrm{S}(\tau)$, and take its average over all intervals.In a surface with true fractal features, the rescaled range should satisfy the scaling form

$$R_{\mathrm{S}}(\tau) = \frac{R(\tau)}{S(\tau)} \sim \tau^{\mathrm{H}} \tag{13}$$

where H is the Hurst exponent. A typical curve obtained from the Hurst analysis of a signal is shown in Fig. 4a.

DFA

The DFA [8] aims to improve the evaluation of correlations in a time series by eliminating linear trends in the data. The method consists initially in obtaining a new integrated series

$$\tilde{z} = \sum_{k=1}^{i} \left(z_k - \langle z \rangle\right) \tag{14}$$

the average $\langle z \rangle$ being taken over all N points,

$$\langle z \rangle = \frac{1}{n}\sum_{i=1}^{N} z_i \tag{15}$$

After dividing the series into intervals of size τ, the points inside a given interval are fitted by a straight line. Then a detrended-variation function Δ_i is obtained by subtracting from the integrated date the local trend as given by the fit. Explicitly, we define

$$\Delta_i = \tilde{z}_i - h_i \tag{16}$$

in which h_i is the value associated with point i according to the fit. Finally, we calculate the root-mean-square fluctuation $F(\tau)$ inside an interval as

$$F(\tau) = \sqrt{\frac{1}{\tau}\sum_{i} \Delta_i^2} \tag{17}$$

and average over all intervals. For a true fractal surface, $F(\tau)$ should behave as

$$F(\tau) \sim \tau^{\alpha}, \tag{18}$$

where α is the scaling exponent. A typical curve obtained from the DFA of a signal is shown in Fig. 4b.

Minimal-cover analysis

This method has been recently introduced [9], and it relates the minimal area necessary to cover a given plane curve, in a specified scale, to a power law behaviour. The scale is introduced by dividing the domain of definition of the function in n intervals of width τ. In each interval j ($1 \leq j \leq n$) we can associate a rectangle of base and height A_j, defined as

$$A_j = \max\{y_i \in [j, j+\tau]\} - \min\{y_i \in [j, j+\tau]\} \tag{19}$$

such that the minimal area will be given by

$$S(\tau) = \sum_{j=1}^{n} \tau A_j \tag{20}$$

In the scaling region, $S(\tau)$ should behave as

$$S(\tau) \sim \tau^{1-\mu} \tag{21}$$

where μ measures the fractality of the curve and is equal to zero when the signal presents no fractality.A typical curve obtained from the minimal-cover analysis of a signal is shown in Fig. 4c.

Box-counting analysis

The box-counting dimension, which is one of the best known fractal dimensions [10], is easily defined and obtained numerically. It can be introduced in a general d-dimensional euclidean space, where a hyper-volume is embedded, by considering the number of hypercubes of side length τ, $N(\tau)$, necessary to cover the entire volume. For a real fractal, $N(\tau)$ should follow the power law

$$N(\tau) \sim \tau^{-D_B}$$

where D_B is the box-counting fractal dimension.

For non-fractal objects, this dimension corresponds to the topological dimension and, in particular, for continuous planar curves D_B is equal to 1.

A typical box-counting curve for a signal is shown in Fig. 4d.

Results and discussion

The PCA and KL transformation of the vectors obtained from the renormalized hysteresis cycle, given by Eq. 1, are shown in Figs. 5 and 6, respectively. The components of the vectors correspond to the amplitudes of the renormalized magnetization at equally spaced field values and have been obtained by linear and spline interpolation procedures. In the numerical treatment we have considered vectors with 187 components, which correspond to the number of experimental points of each branch of the hysteresis loop, and the number of loops for each sample were 12, 10, 06 and 05, corresponding to classes A, B, C and D, respectively.

The results obtained with linear interpolation are presented in Figs. 5a and 6a, whereas the ones with spline interpolation are presented in Figs. 5b and 6b, respectively. As we can see, although the results are not sensitive to the interpolation procedure, a great improvement is achieved by applying KL transformation.

These conclusions can also be also verified by looking at the numerical results which are presented in Tables 2 and 3, obtained by using PCA, and in Tables 4 and 5 obtained by using KL transformation. As mentioned above, the results are insensitive to the interpolation method used; however, a remarkable improvement is reached with the application of KL transformation, when a 100% success classification rate has been reached.

A further improvement in the results can be obtained by preprocessing the signals built with the amplitudes of the

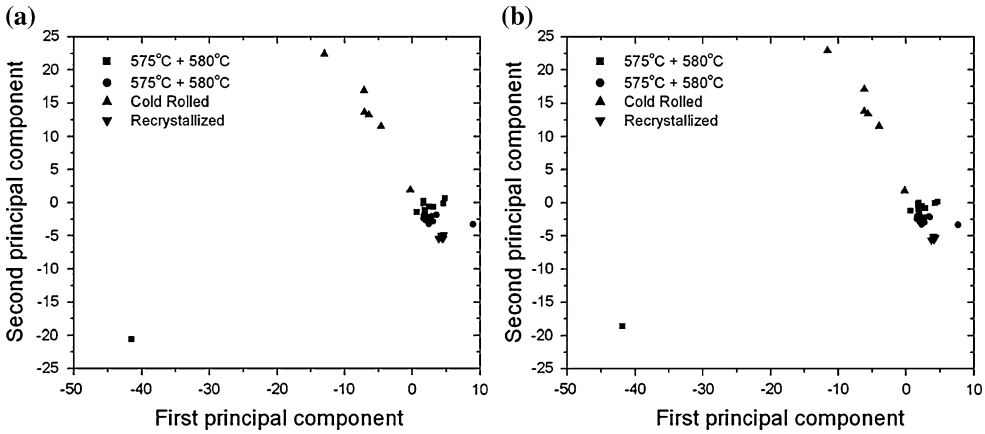

Fig. 5 PCA of the vectors obtained from Eq. 1 by linear interpolation (**a**) and by spline interpolation (**b**) of the data

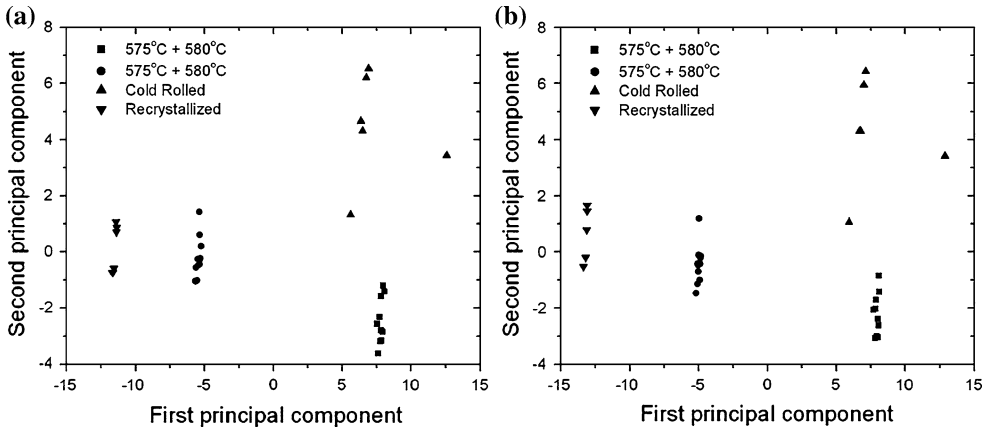

Fig. 6 KL transformation of the vectors obtained from Eq. 1 by linear interpolation (**a**) and by spline interpolation (**b**) of the data

Table 2 Confusion matrix for the training vectors obtained by applying the nearest-class-mean rule to the results of PCA of the vectors defined in Eq. 1 by linear interpolation of the data

	575 + 580 °C	600 + 620 °C	Cold rolled	Recrystallized
575 + 580 °C	10	0	16.67	0
600 + 620 °C	90	100	0	0
Cold rolled	0	0	83.33	0
Recrystallized	0	0	0	100

Table 3 Confusion matrix for the training vectors obtained by applying the nearest-class-mean rule to the results of PCA of the vectors defined in Eq. 1 by spline interpolation of the data

	575 + 580 °C	600 + 620 °C	Cold rolled	Recrystallized
575 + 580 °C	10	0	16.67	0
600 + 620 °C	90	100	0	0
Cold rolled	0	0	83.33	0
Recrystallized	0	0	0	100

Table 4 Confusion matrix for the training vectors obtained by applying the nearest-class-mean rule to the results of KL transformation of the vectors defined in Eq. 1 by linear interpolation of the data

	575 + 580 °C	600 + 620 °C	Cold rolled	Recrystallized
575 + 580 °C	100	0	0	0
600 + 620 °C	0	100	0	0
Cold rolled	0	0	100	0
Recrystallized	0	0	0	100

Table 5 Confusion matrix for the training vectors obtained by applying the nearest-class-mean rule to the results of KL transformation of the vectors defined in Eq. 1 by spline interpolation of the data

	575 + 580 °C	600 + 620 °C	Cold rolled	Recrystallized
575 + 580 °C	100	0	0	0
600 + 620 °C	0	100	0	0
Cold rolled	0	0	100	0
Recrystallized	0	0	0	100

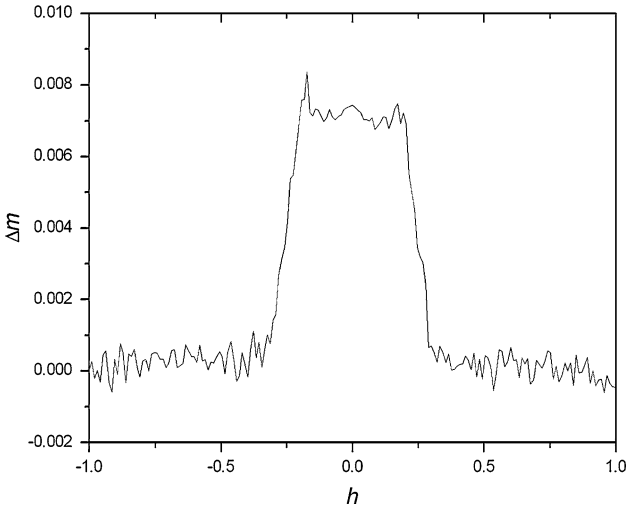

Fig. 7 Renormalized magnetization amplitude $(\Delta m = m^{+}(h) - m^{-}(h))$ as a function of renormalized field h

renormalized magnetization as a function of the renormalized magnetic field. A typical signal is shown in Fig. 7, and in the preprocessing by using fractal and statistical fluctuation analyses, we will construct vectors with 19 components. As already mentioned, these vectors are obtained by using Eqs. 12, 17 and 20 for Hurst, DFA and minimal-cover analyses, respectively, and by using the definition of $N(\tau)$ for box-counting analysis.

The results for the PCA and KL transformation of the vectors obtained by the preprocessing through DFA, and by linear interpolation of the data, are shown in Figs. 8 and 9,

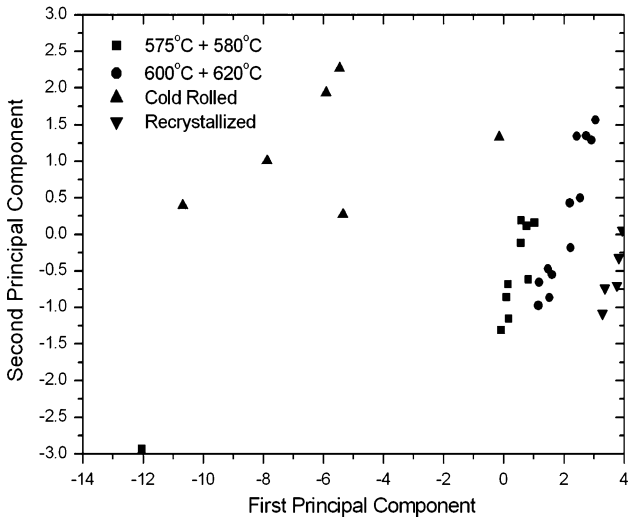

Fig. 8 PCA of the vectors obtained by DFA (Eq. 17) of linear interpolation of the data

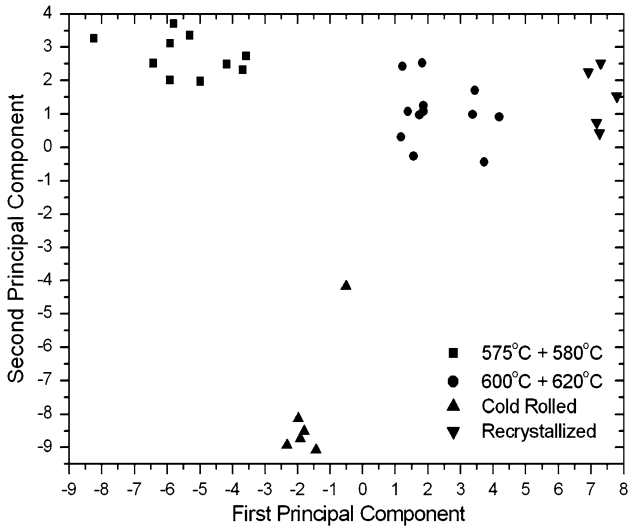

Fig. 9 KL transformation of the vectors obtained by DFA (Eq. 17) of linear interpolation of the data

respectively. As in the previous analysis, without preprocessing, a remarkable improvement has been reached by the application of the KL transformation. It also should be noted that the DFA preprocessing has also greatly improved the results obtained with PCA.

The numerical results obtained for the different preprocessing using PCA and KL transformation are shown in Tables 6 and 7, respectively. These numerical results confirm the previous conclusion that the best classification has been reached by using DFA analysis in the preprocessing of the signals associated with KL transformation and, in this case, a 100% success classification rate has been achieved.

Table 6 Percentage of vectors correctly classified by applying the nearest-class-mean rule to the results of PCA of the vectors obtained by different fluctuation and fractal analyses of linear interpolation of the data

	Hurst	DFA	Minimal cover	Box counting
575 + 580 °C	60	60	30	20
600 + 620 °C	33.33	100	50	66.67
Cold rolled	100	83.33	83.33	100
Recrystallized	80	100	60	100

Table 7 Percentage of vectors correctly classified by applying the nearest-class-mean rule to the results of KL transformation of the vectors obtained by different fluctuation and fractal analyses of linear interpolation of the data

	Hurst	DFA	Minimal cover	Box counting
575 + 580 °C	100	100	100	90
600 + 620 °C	91.67	100	91.67	66.67
Cold rolled	100	100	100	100
Recrystallized	100	100	100	100

Conclusions

In this article, we have looked at the evolution of the recrystallization of a cold rolled non-oriented electric steel through the fluctuation and fractal analyses of the magnetic hysteresis loops associated with two pattern classification techniques, PCA and KL transformation. Due to the small number of experimental data, the classification scheme has been restricted to consider all samples to the training set.

These techniques have been initially applied to vectors whose components have been built with the amplitudes of the renormalized magnetization in the renormalized hysteresis loops at equally spaced renormalized magnetic fields. For these vectors, the results have not been sensitive to the interpolation procedures and, although a 100% success classification rate has been achieved with the KL transformation, a poor result has been obtained by using PCA.

By applying the statistical fluctuation (Hurst and DFA) and fractal analyses (minimal-cover and box-counting) as preprocessing techniques on the vectors used in the previous calculations, a similar result for the previous one was obtained for pattern classification with KL transformation. However, an improvement has been obtained in the pattern classification when using PCA in particular. This improvement has been especially remarkable when DFA was used as a preprocessing technique.

Although we have obtained excellent results for microstructural classification by looking at the evolution of the hysteresis loops, it should be noted that in the calculations

we considered all loops belonging to the training set and consequently the statistical robustness of the technique has to be validated. This means that we have to consider a testing set for each class and, consequently, it will be necessary a larger number of experimental results.

Acknowledgements This work was partially financed by the Brazilianagencies CNPq, FINEP(CT-PETRO), CAPES and PETROBRÁS (Brazilian Oil Company).

References

1. Sha YH, Zhang F, Zhou SC, Pei W, Zuo L (2008) J Magn Magn Mater 320:393
2. Park JT, Szpunar JA (2003) Acta Mater 51:3037
3. Lancorotte MS, Goldemberg C, Penteado AA Jr (2005) IEE Trans Energy Convers 20:2
4. Webb AR (2002) Statistical pattern recognition, 2nd edn. Wiley, West Sussex
5. Vieira AP, de Moura EP, Gonçalves LL, Rebello JMA (2008) Chaos Solitons Fractals 38:748
6. Moura EP, Vieira AP, Irmão MAS, Silva AA (2009) Mech Syst Signal Process 23:682
7. Hurst HE (1951) Trans Am Soc Civ Eng 116:770
8. Peng CK, Buldyrev V, Havlin S, Simmons M, Stanley HR, Goldberger AL (1994) Phys Rev E 49:1685
9. Dubovikov MM, Starchenko NV, Dubovikov MS (2004) Physica A 339:591
10. Addison PS (1997) Fractals and Chaos. IOP, London